Soft Matter

PAPER

View Article Online
View Journal | View Issue

Cite this: *Soft Matter*, 2024, **20**, 7723

Model to rationalize and predict the formation of organic patterns originating from an enzyme-assisted self-assembly Liesegang-like process of peptides in a host hydrogel†

Jean-Yves Runser,‡[abc] Shahaji H. More,‡[abc] Fatima Fneich,[def] Timothée Boutfol,[c] Pierre Weiss,[def] Marc Schmutz,[c] Bernard Senger,[ab] Loïc Jierry *[c] and Pierre Schaaf*[abc]

Received 20th July 2024,
Accepted 16th September 2024

DOI: 10.1039/d4sm00888j

rsc.li/soft-matter-journal

Recently, we have investigated the enzyme-assisted self-assembly of precursor peptides diffusing in an enzyme-containing host gel, leading to various self-assembly profiles within the gel. At high enzyme concentrations, the reaction–diffusion self-assembly processes result in the formation of a continuous non-monotonous peptide self-assembly profile. At low enzyme concentrations, they result in the formation of individual self-assembled peptide microglobules and at intermediate enzyme concentrations both kinds of self-assembled structures coexist. Herein, we develop a Liesegang-type model that considers four major points: (i) the diffusion of the precursor peptides within the host gel, (ii) the diffusion of the enzymes in the gel, (iii) the enzymatic transformation of the precursor peptides into the self-assembling ones and (iv) the nucleation of these building blocks as the starting point of the self-assembly process. This process is treated stochastically. Our model predicts most of the experimentally observed features and in particular (i) the transition from a continuous to a microglobular pattern of self-assembled peptides through five types of patterns by decreasing the enzyme concentration in the host hydrogel. (ii) It also predicts that when the precursor peptide concentration decreases, the enzyme concentration at which the continuous/microglobules transition appears increases. (iii) Finally, it predicts that for peptides whose critical self-assembly concentration in solution decreases, the peptide concentration at which the continuous-to-microglobular transition decreases too. All these predictions are observed experimentally.

Introduction

In 2004, Bing Xu introduced an approach commonly known as enzyme-assisted self-assembly (EASA) which was mainly illustrated over the last two decades through the self-assembly of short peptides or peptide-like sequences.[1] It consists of a biomimetic approach where peptide precursors are brought into contact with enzymes that transform the peptides into self-assembling entities. When the concentration of these building blocks exceeds a critical concentration (CC) characteristic of the molecular structure of the precursor, the peptide self-assembly starts leading to nanostructures. EASA processes taking place in solution have received great attention and many of their specific features were established, despite some fundamental points still to address.[2] Of particular interest for the present work, is the initiation of the peptide self-assembly by a nucleation mechanism requiring a concentration exceeding the CC of the peptides as indicated above.[2,3] Compared to other triggers of peptide self-assembly, enzymes offer the possibility to spatially control the self-assembly through their prior localization. This localized EASA approach (called LEASA) was described for the first time in 2009 by Ulijn and coworkers through the covalent immobilization of enzymes onto a glass substrate, resulting in the formation of self-assembled peptide nanostructures growing exclusively in a bottom–up approach from the substrate.[4] This 2D localization of the growth of peptide self-assembly was used to design nanomaterials,[5] biomaterials

[a] *Institut National de la Santé et de la Recherche Médicale, INSERM Unité 1121, CRBS, 1 rue Eugène Boeckel, CS 60026, 67084 Strasbourg Cedex, France. E-mail: schaaf@unistra.fr*
[b] *Université de Strasbourg, Faculté de Chirurgie Dentaire, 8 rue Sainte Elisabeth, 67000 Strasbourg, France*
[c] *Université de Strasbourg, CNRS, Institut Charles Sadron (UPR22), 23 rue du Loess, 67034 Strasbourg Cedex 2, BP 84047, France. E-mail: ljierry@unistra.fr*
[d] *Université de Nantes, ONIRIS, INSERM UMR 1229, 1 place Ricordeau, Nantes, 44042, France*
[e] *UFR Odontologie, Université de Nantes, 44042, France*
[f] *CHU Nantes, PHU4 OTONN, Nantes, 44042, France*

† Electronic supplementary information (ESI) available. See DOI: https://doi.org/10.1039/d4sm00888j

‡ Both authors contributed equally.

coating,[6] magneto-sensitive materials,[7] catalytically active supported hydrogels[8] as examples of applications.[3,9] Since cells, organelles or bacteria localize enzymes at interfaces in living systems, self-assembly of peptides can thus be initiated at specific areas resulting in impressive biomedical developments.[10]

Reaction–diffusion processes to get patterned materials are a powerful approach.[11] However, spatiotemporal self-assembly of organic building blocks in a 3D environment through reaction–diffusion processes are still rare although emerging since a few years. In a pioneer work published in 2017, the Eelkema and van Esch groups have shown that two complementary precursor solutions diffusing one to the other through a polymer hydrogel interact spontaneously, resulting in self-assembled nanostructures and a patterning of the host polymer hydrogel.[12] Various parameters can thus be used to finely tune the self-assembled pattern features in a spatiotemporal way.[13] These organic self-assembled nanostructures can also be locally generated at the interface between two distinct hydrogel pieces containing complementary precursors: in this case, the formation of the self-assembling compounds at the interface leads to nanofibril structures interpenetrating both hydrogel pieces and playing thus the role of a glue between them.[14] Currently, only a few contributions are dedicated to the behavior of self-assembling species at gel–gel[15] or at liquid–gel interfaces.[16] It is well known that protons are effective triggers of low-molecular-weight hydrogelators self-assembly with both a spatial and temporal resolution.[17] Hermans and Besenius localized the pH-triggered self-assembly of benzene-1,3,5-tricarboxamide on the surface of poly(dimethylsiloxane) cubes soaked previously in HCl to induce slow proton diffusion out of the material.[18] Recently, Smith and coworkers succeeded in designing dynamic multi-domains of various self-assembled hydrogels: proton diffusion from a reservoir located in a self-assembled gel directs the self-assembly of a pH-responsive hydrogelator within this self-assembled matrix[19] or out of it.[20] In addition, the control of this proton diffusion allows to get patterned and shaped hydrogels. The nature of the proton source and the addition of agarose impact the resulting 3D pattern in the host material.[21]

In 2019, we showed that the spatial control of the peptide self-assembly process can also be performed in 3D using EASA[22] by functionalizing the gels with free enzymes,[23] or enzyme-grafted on silica nanoparticles,[24] and then by letting the precursor peptides diffuse within these enzyme-containing host materials. One great difference between self-assembly processes taking place in solution compared to those taking place in gel is that the self-assembled structures are stuck in the gel whereas this is only the case when a gelation point is reached in solution. This strongly influences the outcome of the reaction–diffusion self-assembly processes.

Previous experimental observations and ongoing processes

In previous studies, we and others have investigated the tripeptide Fmoc-FF*p*Y (Fmoc: fluoromethylmethoxycarbonyl, F: phenylalanine; Y: tyrosine; p: phosphate group)[25,26] diffusing into a silanized hydroxypropylmethylcellulose (Si-HPMC) host gel that contains free alkaline phosphatase (AP) enzymes. In the presence of AP, the precursor peptide Fmoc-FF*p*Y transforms into the hydrogelator peptide Fmoc-FFY that, above a critical concentration, self-assembles into peptide aggregates. When investigating carefully this precursor/hydrogelator system, we found that it does not result in the formation of a monotonous distribution of self-assembly but rather in a profile presenting two or more self-assembly areas, spatially well defined.[27] When decreasing the enzyme concentration in the gel, the continuous peptide self-assembly profile is gradually replaced by isolated peptide self-assembled microglobules randomly distributed over the gel.[28] These features were explained by a mechanism related to that involved in the inorganic patterning observed in hydrogels and called Liesegang ring structures.[29] As soon as a precursor peptide solution is brought into contact with an enzyme functionalized host gel, some enzymes diffuse out from the host gel into the solution. These enzymes that have diffused in the solution are transforming a part of the precursor peptides into self-assembling species at the interface (Fig. 1, step a, the blue line shows the self-assembling peptide concentration). This is at the origin of the maximum of self-assembled peptides observed at the gel/solution interface (Fig. 1, step b, green line). However, precursor peptides from the solution do not all transform into self-assembling species located at the interface. Some of the precursors diffuse within the gel where they are transformed by the enzymes still embedded in the gel. The self-assembly of the hydrogelators requires locally a concentration of about CC or more. As long as this concentration is insufficient within the host gel, these self-assembling species are freely diffusing. Some of them diffuse towards the first self-assembly maximum located at the gel/solution interface where they are incorporated into the already formed self-assembled peptide structure. This behavior creates a zone, in the gel, around the gel/solution interface, which is depleted in self-assembling species. Thus, in this zone, the concentration CC can never be reached. Further from the interface (more in-depth in the host hydrogel), the concentration of self-assembling species increases due to its enzymatic production from precursors. In this region, the critical concentration CC can thus be reached and the self-assembly starts through a nucleation and growth mechanism (Fig. 1, step c). This phenomenon repeats deeper in the gel and results in a second self-assembly maximum (Fig. 1, step d). This self-assembly area grows and, similarly to the growth of the first maximum, it induces a decrease of the concentration of self-assembling species around it. When the initial concentration of precursor peptides in the solution is high enough,[27] some of these peptides continue to diffuse even further into the gel and through a similar process, a third self-assembly maximum can eventually be built up deeper in the gel.

When a low enzyme concentration is initially present in the host gel, some enzymes still diffuse into the solution. As soon as the precursor peptide solution is deposited, the contact of the Fmoc-FF*p*Y peptide with this enzyme leads

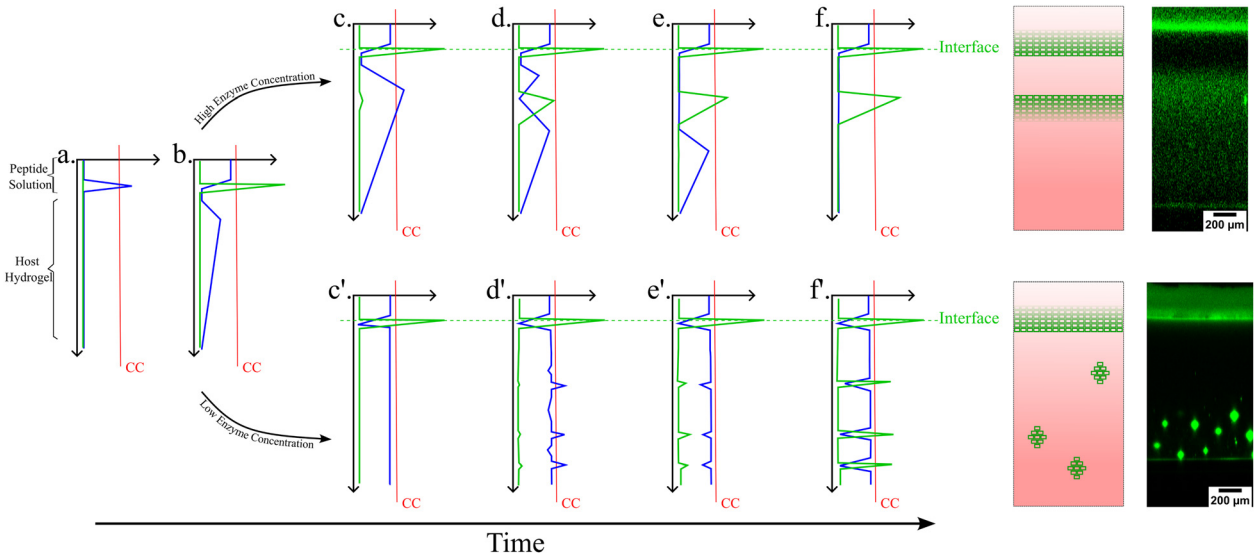

Fig. 1 Schematic representation of typical Liesegang-like patterns observed from the diffusion of a precursor peptide within an enzyme-encapsulating host gel.[27,28] Two different pathways, steps (c)–(f), and steps (c′)–(f′), are shown according to the high or low enzyme concentration in the host gel, respectively. The blue line corresponds to the self-assembling peptide concentration as a function of position from the top of the solution down to the bottom of the gel. The green line corresponds to the self-assembled peptides concentration. The straight red line represents the CC of the self-assembling peptide beyond which the self-assembly and then the patterning occurs.

again to a self-assembly maximum at the gel/solution interface (Fig. 1, steps a, b). The difference with the case of a high enzyme concentration distributed all over the volume of the host gel is that the enzymatic transformation of precursor peptides into self-assembling species is now slower (Fig. 1, step c′). Although the self-assembly maximum at the gel/solution interface acts again as a sink (or an ''attractor'') for the self-assembling species in its close vicinity, their concentration presents again a maximum somewhere in the gel. But now, the concentration at this maximum increases slowly with time because of the lower concentration of enzymes. When it approaches CC, density fluctuations initiate locally the self-assembly process (Fig. 1, step d′). The slower the increase of the hydrogelator concentration, the more likely a ''giant'' fluctuation has time to take place and to initiate locally the self-assembly process (Fig. 1, step e′). This local self-assembly then attracts the self-assembling species diffusing in its surrounding environment, decreasing locally their concentration and thus preventing further self-assembly around it. When the rate of increase of the hydrogelator concentration is small, there is enough time for a giant concentration fluctuation to appear. This fluctuation generates one microglobule. Peptides around this microglobule have time to diffuse towards it and self-assemble onto it before new fluctuations in its vicinity take place. This leads to a zone depleted in hydrogelators (Fig. 1, step f′). In the case where the rate of increase of the concentration of self-assembling peptides is faster without being too fast, density fluctuations and small self-assembled microglobules will appear simultaneously. One then observes isolated microglobules in a continuous self-assembled structure pattern.[28] At high precursor concentrations, the increase of the hydrogelator concentration is so rapid that small fluctuations appear everywhere and initiate the self-assembly, leading to the continuous self-assembly pattern discussed above.

A schematic describing the different steps a to f/f′ (Fig. 1) of the peptide (*i.e.* Fmoc-FFY) self-assembled pattern formation is given in Fig. S1 of the ESI.†

Previously, we established a deterministic model based on reaction–diffusion processes including many features of the EASA process in host gels leading to continuous self-assembly profiles using high enzyme concentration as mentioned above.[27] Though, this model was unable to predict the transition from the continuous to microglobular self-assembled peptides area in the case of low enzyme concentration embedded in the host gel. By extending the reaction–diffusion model to take the stochastic nature of the self-assembly initiation into account, we could explain the appearance of microglobules in a homogeneous system in which the concentration of self-assembling species grows uniformly in space at a slow rate.[28] For a high rate of self-assembling species formation, the model predicts a continuous self-assembly in space. But a single and general model that should capture most of the experimental observations in the continuous self-assembly regime and predict the continuous-microglobule transition had to be developed. This is done in this paper. Experimental and simulated peptide self-assembled patterns observed within the host hydrogel when enzyme or precursor peptide concentration change are compared and discussed. The robustness of the model is also evaluated by changing the volume of the precursor peptide solution deposited onto the enzyme-embedded host hydrogel or the critical self-assembly concentration by changing the nature of the peptide.

Material and methods

Material

Alkaline phosphatase (AP) from bovine intestinal mucosa (10 DEA units mg^{-1} protein, 160 kDa), *para*-nitrophenyl phosphate (PNPP), Hepes buffer and Thioflavine T (ThT) were purchased from Sigma Aldrich. Sodium tetraborate anhydrous (Borax) was supplied by Acros Organics. Fmoc-*p*Y (99% purity, natural chirality) was purchased from Iris Biotech. Fmoc-FF*p*Y and Fmoc-FFF*p*Y (Fig. 2a) were synthesized according to procedure described in ESI,† and their characterizations were identical to that reported in a previous work (in case of Fmoc-FF*p*Y).[30] AP^{RHO} was prepared according to the literature (RHO stands for rhodamine B).[31] HA (PrimaHyal®) M_w 406 000 g mol^{-1}, (polydispersity 1.574) was obtained from Givaudan. Si-HPMC and Si-HA were prepared following the described procedures.[32,33]

Finally, one can point out that we call these processes "Liesegang-like" processes because they result from diffusion/reaction processes involving a nucleation process that takes place only when the CC of one of the compounds is attained. However, there are also differences with the mechanism leading to "classical" Liesegang patterns. The EASA process relies on the enzymatic transformation of its substrate but does not involve the enzyme in the resulting product. In contrast in the classical Liesegang process the two partners react and are consumed.

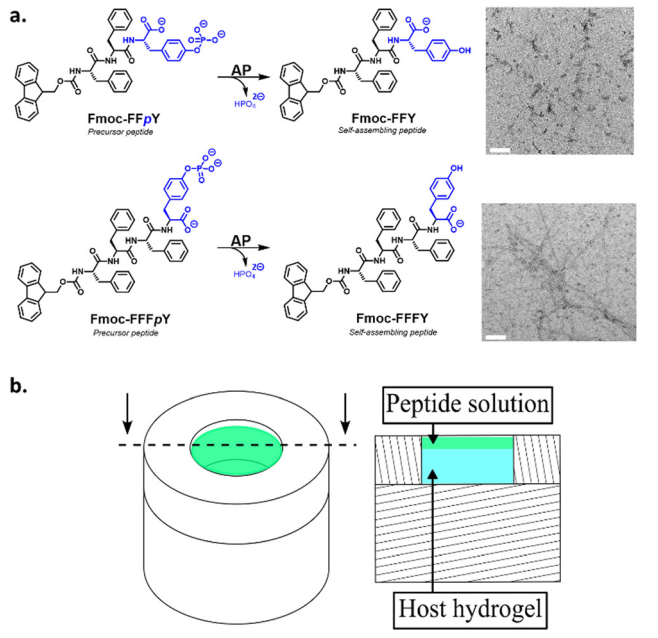

Fig. 2 (a) AP catalyzes the phosphate hydrolysis of the amphiphilic precursor peptides Fmoc-FF*p*Y or Fmoc-FFF*p*Y to their corresponding Fmoc-FFY or Fmoc-FFFY self-assembled nanofibers, respectively. The blue color highlights the hydrophilic part of the peptides. Typical TEM images of each resulting nanostructures are given (white scale bars indicate 100 nm). (b) 3D (left) and sectional drawing (right) of the Teflon mold containing the AP-HPMC host gel (cyan colour) and the peptide solution (green colour) deposited on its top.

Methods

Preparation of 1.5% w/v AP-HPMC and diffusion of Fmoc-FF*p*Y or Fmoc-FFF*p*Y within the host hydrogel. Silanized hydroxypropylmethylcellulose (Si-HPMC) was prepared according to reported methods.[32] HPMC hydrogels were obtained after mixing 100 μL of a Si-HPMC solution at 3% w/v in NaOH 0.1 M and pH 12.9 with 100 μL of HEPES buffer at pH 3.6 under mechanical stirring. The gelation occurred at room temperature. The encapsulation of AP or rhodamine-labeled AP (AP^{RHO}) in these gels is done by dissolving AP or AP^{RHO} in the HEPES buffer before mixing it with Si-HPMC solution at 3% w/v. For the Fmoc-FF*p*Y diffusion tests, after 48 h gelation, 50 μL of Fmoc-FF*p*Y solution (at the desired concentration in borax buffer 25 mM, pH 9.5) was added on top. These 50 μL diffused into the host hydrogel for 24 h before further investigations.

Preparation of 3% w/v Si-HA and diffusion of Fmoc-FF*p*Y within the host hydrogel. Silanized hyaluronic acid (Si-HA) was prepared according to reported methods.[33] Briefly, HA hydrogels were obtained after mixing 160 μL of a Si-HA solution at 3.75% w/v in NaOH 0.1 M and pH 12.9 with 40 μL of HEPES buffer at pH 2.1 under mechanical stirring. The gelation occurred at room temperature and led to a hydrogel at 3% w/v of final Si-HA concentration, having 15–76 nm of mesh size. The encapsulation of AP in these gels is done by dissolving AP in the HEPES buffer before mixing it with the Si-HA solution at 3.75% w/v. For the Fmoc-FF*p*Y diffusion tests, after 48 h gelation, 50 μL of Fmoc-FF*p*Y solution (at 2 mg mL^{-1} in borax buffer 25 mM, pH 9.5) was added on top. These 50 μL diffused into the host hydrogel for 24 h before further investigations (revelation of self-assembly by CLSM in particular, was ensured by addition of a solution of ThT (0.1 mg mL^{-1} in borax buffer) on top of the hydrogel 2 h before imaging).

Monitoring by confocal laser scanning microscopy (CLSM). Host hydrogels were prepared in 10-mm diameter Teflon molds (Fig. 2b) by mixing 100 μL of Si-HPMC solution at 3% w/v in NaOH (0.1 M, pH 12.9) with 100 μL of HEPES ((4-(2-hydroxyethyl)-1-piperazineethanesulfonic acid)) buffer at pH 3.6 through mechanical stirring. The gelation process takes place for 48 h. The encapsulation of AP (AP or a mixture of AP and AP^{RHO} called AP/AP^{RHO}) in these host hydrogels was ensured by dissolving AP in HEPES buffer. The reticulation process took place over 48 h and resulted in a host hydrogel containing AP (AP-HPMC or AP^{RHO}-HPMC) ready for further experiments. At this point 50 μL of Fmoc-FF*p*Y (at the desired concentration) were added on top of the host hydrogel. This solution of peptide stayed in contact with the host hydrogel for 24 h at room temperature, and the interface with the hydrogel never dried. The revelation of self-assembly by confocal imaging was ensured by addition of a solution of ThT (0.1 mg mL^{-1} in borax buffer) on top of the hydrogel 2 h before imaging.[28] In the case of kinetic experiments, ThT was also dissolved in HEPES buffer prior to the construction of the host hydrogel. Confocal laser scanning microscopy (CLSM) images were captured with a Zeiss LSM 710 microscope using a EC Plan-Neofluar 10×/0.3 objective. The fluorescence of rhodamine B was measured with an excitation wavelength of 561 nm and emission wavelength

between 565 and 700 nm. The fluorescence of Thioflavine T was measured with excitation by an argon laser with a cut-off dichroic mirror at 458 nm and an emission band-pass filter between 460 and 550 nm.

Transmission electron microscopy (TEM). First, supramolecular hydrogels based on self-assembled Fmoc-FFY and Fmoc-FFFY nanofibers were prepared as follows: 50 μL solution of AP at 3 mg mL^{-1} in borax buffer (25 mM, pH 9.5 from sodium tetraborate anhydrous in ultrapure water), 50 μL solution of Fmoc-FF*p*Y or Fmoc-FFF*p*Y at 15 mg mL^{-1} in borax buffer and finally 50 μL of borax buffer solution were mixed together and then vortexed for 5 s. Then, samples were kept without stirring at room temperature. Once hydrogels are observed, they are vortexed to get a solution, diluted with borax buffer up to 500 times. 20 μL of the diluted solution was dropped off on a shelf and observed using a TEM Technai G2 microscope after negative staining. To make the observations, 5 μL of each solution (*i.e.* Fmoc-FFY or Fmoc-FFFY) were deposited onto a freshly glow discharged carbon-covered grid (400 mesh). The solution was left for 1 min and the grid was negatively stained with 5 μL of uranyl acetate (2% in water) for another minute and finally dried using a filter paper. The grids were observed at 200 kV with a Tecnai G2 (FEI) microscope. Images were acquired with a camera Eagle 2k (FEI) ssCCD camera.

Determination of the critical concentration (CC) of self-assembly. To determine the CC for the self-assembly of Fmoc-FFY and Fmoc-FFFY generated *in situ* in presence of AP from their corresponding phosphorylated precursors Fmoc-FF*p*Y and Fmoc-FFF*p*Y, respectively, a fluorescence monitoring was done over time using an automated multiplate reader (FLX-Xenius, SAFAS, Monaco). First, we prepared two concentration series of both precursor peptides Fmoc-FF*p*Y and Fmoc-FFF*p*Y ranging respectively from 1 mg mL^{-1} (1.3 mM) to 1.95×10^{-3} mg mL^{-1} (2.5×10^{-3} mM) and from 1.2 mg mL^{-1} (1.3 mM) to 2.34×10^{-3} mg mL^{-1} (2.5×10^{-3} mM) (in 25 mM borax buffer, pH 9.5). Then, we put 100 μL of each of these peptide solutions in a 96-well plate as well as 100 μL of a solution containing ThT at 0.01 mg mL^{-1} and AP at 0.5 mg mL^{-1} (in 25 mM borax buffer, pH 9.5). Thus, we had in each well final ThT and AP concentrations of 0.005 mg mL^{-1} and 0.25 mg mL^{-1}, respectively. The final range of peptide concentrations was also divided by two ranging from 6.5×10^{-1} mM down to 6.5×10^{-4} mM. Since ThT becomes fluorescent in presence of β-sheet self-assembled peptide structures,[28] it allowed us to determine the minimum CC required for each dephosphorylated peptide, *i.e.* Fmoc-FFY and Fmoc-FFFY, to self-assemble. Results are provided in Fig. S2 in ESI.†

Simulations. Simulations were performed using a home-made computer code written in python. The script of the program is given in ESI† (Part 6). In this program, equations described in the section "Mathematical model" are solved using the finite element method.

Mathematical model. The model that we have developed belongs to the family of "pre-nucleation" models.[34] It relies on reaction/diffusion reactions. The different processes going on and their relationship with the model presented here below are schematically represented in Fig. S1 of ESI.† These were first solved in a pure "deterministic" way by neglecting both fluctuations and the stochastic nature of the chemical reactions and nucleation process. However, since the mid 1990th it was recognized that fluctuations in the diffusion processes and stochasticity of the reactions have to be introduced to account for all the observations. The first to introduce fluctuations into their mathematical description were Chopard *et al.* who developed a cellular automata model.[35,36] Later, Antal *et al.* used a kinetic Ising model to include noise through a probabilistic description of the transition between discrete states of the system.[37] Lagzi introduced fluctuations into the diffusion term and Grzybowski, Epstein and others accounted for the stochasticity by including stochastic functions in the term corresponding to the chemical reactions producing the precipitating species.[38–42] By varying a parameter from 0 to 1 they could tune the degree of stochasticity from purely deterministic to purely probabilistic. We have chosen to introduce stochasticity through the term describing the nucleation process. This allows to describe the transition from a continuous self-assembly profile to an assembly of globules randomly distributed in the host gel.

The experiments are performed as follows: a host gel functionalized with enzymes (*i.e.* AP-HPMC) is brought in contact with a solution containing the peptide precursor (*i.e.* Fmoc-FF*p*Y) solution. In the following, the self-assembling peptides are called hydrogelator peptides (*i.e.* Fmoc-FFY) as mentioned before. We will note O_x the axis perpendicular to the gel/solution interface. The solution corresponds to x between 0 and x_i, and the gel to x between x_i and x_f. We will denote the concentration of precursor peptides c_{PP}. The enzymes, *i.e.* AP, are free to diffuse in the gel. We will denote the concentration of free diffusing enzymes by c_E. The initial condition on the precursor peptides is that $c_{PP}(x, t = 0) = c_{PP0}$ for $0 \leq x \leq x_i$ and $c_{PP}(x, t = 0) = 0$ for $x > x_i$. The initial enzyme profile is defined by

$$c_E(x, t = 0) = c_{E0}\left(1 - \exp\left(-\frac{(x - x_0)}{x_1}\right)\right) \quad (1)$$

for $0 \leq x \leq x_f$ and $c_E(x, t = 0) = 0$ otherwise, with $x_0 < x_i$ and $x_1 > 0$. This profile is somewhat arbitrary but should reflect the experimental observations that when the precursor peptide solution is brought in contact with the host hydrogel, some enzymes are almost instantaneously present (at the time scale of our observation) in the solution creating a depletion of enzymes in the gel near the gel/solution interface (this corresponds to $x_0 < x_i$). The profile resembles a diffusion profile, but the enzyme concentration nowhere reaches zero in the gel (Fig. S3 in ESI†). Once the gel is brought in contact with the precursor peptide solution, a set of diffusion–reaction processes take place in the system which can be translated mathematically into eqn (2)–(6):

$$\frac{\partial c_{PP}}{\partial t} = -k_E(c_E + c_{EF}) \cdot c_{PP} + D_{PP}\Delta c_{PP} \quad (2)$$

$$\frac{\partial c_{PH}}{\partial t} = D_{PH}\Delta c_{PH} + k_E(c_E + c_{EF})\cdot c_{PP} - k_a \cdot c_{PH}\cdot r(c_{PH}) - k_{as}\cdot c_{PH}\cdot c_{PA} + k_{ad}\cdot c_{PA} \quad (3)$$

$$\frac{\partial c_{PA}}{\partial t} = k_a \cdot c_{PH}\cdot r(c_{PH}) + k_{as}\cdot c_{PH}\cdot c_{PA} - k_{ad}\cdot c_{PA} \quad (4)$$

$$\frac{\partial c_E}{\partial t} = D_E\Delta c_E - k_{ea}\cdot c_{PA}\cdot c_E + k_{ed}\cdot c_{EF} \quad (5)$$

$$\frac{\partial c_{EF}}{\partial t} = k_{ea}\cdot c_{PA}\cdot c_E - k_{ed}\cdot c_{EF} \quad (6)$$

eqn (2) is relative to the diffusion of the precursor peptides whose concentration is denoted by c_{PP} and their disappearance due to their enzymatic transformation into hydrogelator peptides (Fig. 2a; concentration of hydrogelator: c_{PH}). D_{PP} represents the diffusion coefficient of the precursor peptides and Δ represents the Laplace operator. k_E represents the enzymatic activity constant. Experimentally it is observed that enzymes diffuse in the gel. Such enzymes are called free enzymes (c_E). But enzymes also adsorb onto peptide self-assemblies. These enzymes are assumed to be fix (c_{EF}) as are the Fmoc-FFY self-assemblies. Both free and bound enzymes are assumed to have the same activity. Eqn (3) describes the evolution of the concentration of hydrogelator peptides whose diffusion coefficient is denoted by D_{PH}. Besides the diffusion and enzymatic formation, when the concentration of hydrogelators exceeds the critical concentration CC, they form self-assembled aggregates by a nucleation process. k_a corresponds to the constant of nucleation and $r(c_{PH})$ is a stochastic function characterizing the nucleation process. The stochasticity of this function takes into account both the stochastic nature of the nucleation process and hydrogelator peptide concentration fluctuations. $r(c_{PH})$ must be a function that is close to zero for $c_{PH} <$ CC and that increases extremely rapidly when c_{PH} exceeds CC. The concentration of hydrogelators that are in an aggregated form (in self-assemblies) is denoted by c_{PA}. k_{as} represents the aggregation constant (addition of a peptide onto an aggregate) and k_{ad} is the disaggregation constant (removal of a peptide from an aggregate). Eqn (4) corresponds to the evolution of the peptide concentrations in self-assembled aggregates. Because it is assumed that self-assembled aggregates are fix in the host-gel, this equation does not contain a diffusion term. Eqn (5) represents the evolution of the concentration of free enzymes. D_E represents their diffusion coefficient, k_{ea} their adsorption constant onto the self-assembled aggregates and k_{ed} the desorption constant of adsorbed enzymes on self-assemblies. The concentration of enzymes that are adsorbed in the self-assembled aggregates is denoted as c_{EF} and its evolution is given by eqn (6). Because these adsorbed enzymes are assumed not to diffuse there is no diffusion term in eqn (6).

These equations were solved by a finite element method both in space and time (Euler method). Moreover, to save computer time, we restrained our simulations to two dimensions. Compared to three dimensions, it does not change the physics of the problem in contrary to a one dimension problem which could impact the resulting solutions. Indeed, in 1D every point on the line divides space in two distinct domains which is not the case in 2 or 3D. The details of the resolution of eqn (2)–(6) are given in ESI† (Part 3). This model incorporates a stochastic function $r(c_{PH})$ which allows a transition from a continuous profile to isolated microglobules when decreasing the enzyme concentration in the host gel. The results presented here were obtained by using the following rules defining $r(c_{PH})$. Over the course of one iteration, *i.e.* one-time step δt, a number u is randomly drawn from a uniform distribution on the interval [0, 1]. Then, we calculate the number:

$$z = \frac{\delta t}{\tau}\cdot \exp\left(\frac{c_{PH} - CC}{P_1}\right) \quad (7)$$

where P_1 sets the sensitivity of z to c_{PH} and τ represents the time unity. If $u < z$ then $r(c_{PH}) = 1$ otherwise $r(c_{PH}) = 0$. Thereby, the greater P_1, the greater the likelihood of nucleation at low concentration of hydrogelators compared to CC. This function takes into account both the effect of c_{PH} fluctuations on the nucleation process and the stochastic nature of the nucleation process itself. The exponential function is aimed at restituting the very strong increase of the nucleation rate as soon as CC is exceeded. However, the precise mathematical expression of z in relation (7) is not of great importance to qualitatively account for the observed trends as long as it is a function that is close to zero for $c_{PH} <$ CC and that increases sharply when $c_{PH} >$ CC. More details and results can be found in ESI† (Fig. S6) concerning this point.

Comparison between experimental peptide self-assembled patterns and model predictions. This part is based on the comparison of new experimental studies, or previously published ones,[27,28] with the general model described above. Hydroxypropylmethylcellulose (HPMC) hydrogel embedding AP, called AP-HPMC, was prepared as described above in the Material and methods section. First, the AP-HPMC host hydrogel was brought into contact with a solution of precursor tripeptides Fmoc-FF*p*Y. In solution, in contact with AP, these amphiphilic phosphorylated tripeptides are enzymatically hydrolyzed leading to self-assembled Fmoc-FFY nanofibers ($\approx$5 nm diameter and several hundred micrometers long), as observed by TEM (Fig. 2a and magnification in Fig. S4 in ESI†).[25,26] The self-assembly of Fmoc-FFY within the host gel was visualized by bringing it in contact with Thioflavine T (ThT) which, when excited at 458 nm, fluoresces in the green spectral window observed by CLSM.[30] The experimental setup that was used is schematically shown in Fig. 2b.

The predictions of the model are sensitive to its parameters as already mentioned by Chopard *et al.* in their modeling of Liesegang patterns of inorganic systems: "*Liesegang patterns are only obtained for a narrow range of parameters and a tedious tuning is necessary to produce them*".[35] The present model is based on a former one that was fully deterministic but already accounted for the non-monotonous self-assembly profile and many parameters entering in the present model were already present in the first one.[27] We thus used these parameters as

starting values for our simulations (Parts 4 and 5, ESI†). Our chemical system is composed of two distinct media: the solution and the gel. One can expect that the diffusion coefficients of the different species, the reaction constants (k_a, k_{as}, k_{ad}, k_E, k_{ea}, k_{ed}), the critical aggregation concentration CC and the parameter P_1 are different in each medium. Experimentally it is observed that, as soon as the gel is brought in contact with the peptide solution, self-assembly starts in the solution at the gel/solution interface. This can be due to a high pulse of enzyme concentration into the solution during contact, to a smaller critical aggregation concentration in the solution than in the gel and/or to a higher enzymatic activity in the solution than in the gel. By exploring the effect of varying multiple parameters on the simulated self-assembly profile it appears that it is crucial that the CC be significantly smaller in the solution than in the gel (Fig. S6 in ESI†). We have thus set CC in the solution to zero. Moreover, this effect can be enhanced by assuming that the enzymatic constant k_E is larger in the solution than in the gel. We have assumed that k_E is 5 times larger in the solution than in the gel. All other parameters are set equal in the solution and in the gel, in particular the different diffusion coefficients.

For a given precursor peptide concentration and by varying the enzyme concentration over four decades, our model is able to reproduce the main features of the experimental observations: indeed, at high enzyme concentration ([AP] = 1 mg mL^{-1}) the self-assembly profile decreases monotonically from the gel/solution interface towards the interior of the host gel (Fig. 3a). We call this a profile of Type I. By decreasing the initial enzyme concentration in the host gel ([AP] = 0.3 mg mL^{-1}) and still keeping the Fmoc-FF*p*Y concentration at 1.2 mg mL^{-1}, a secondary self-assembly maximum appears close to the interface inside the AP-HPMC host gel (Fig. 3b, Type II profile). As we continue to decrease the enzyme concentration further ([AP] = 0.1–0.02 mg mL^{-1}) this secondary maximum migrates from the interface into the AP-HPMC host gel (Fig. 3c, Type III-i profile). As we continue to decrease the enzyme concentration, a minimum of self-assembly corresponding to the depletion zone enlarges and becomes very low. Self-assembled Fmoc-FFY peptide microglobules usually appear within the continuous self-assembly profile in the host gel (Fig. 3d, Type III-ii profile). Finally, when the enzyme concentration becomes very low ([AP] = 0.0025 mg mL^{-1}) only microglobules remain visible in the host gel (Fig. 3e, Type IV).

The observation can be summarized as follows: at high enzyme concentrations nucleation is fast and so results in many nuclei in the zone where CC is reached. Thus, the system on a large scale appears homogeneous over this zone. At low enzyme concentrations, nucleation is slow, only few sites develop, and due to stochasticity, they are randomly distributed in space.

Thus, to sum-up, this evolution of the self-assembly profile is observed experimentally and predicted by the model (Fig. 3a–e). The model also predicts that, in the microglobule regime, there exists a zone in the hydrogel after the interface that is devoid of microglobules. This corresponds to the depletion zone in the

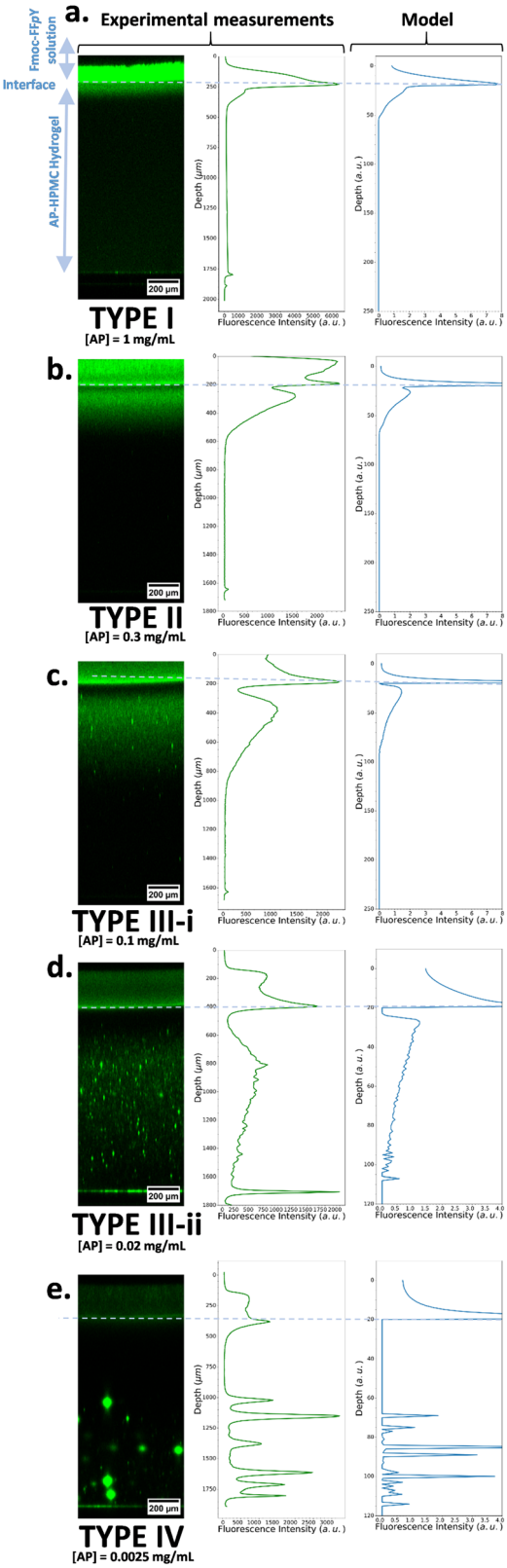

Fig. 3 (left) Experimental CLSM monitoring of the Fmoc-FFY self-assembled pattern revealed by ThT (green emission) within the AP-HPMC gel and its corresponding measured cross-section profiles of the fluorescence emission intensity of ThT (middle). The precursor peptide Fmoc-FF*p*Y concentration is kept at 1.2 mg mL^{-1} and the AP concentration in the host hydrogel is decreased from (a) 1 mg mL^{-1}, to (b) 0.3 mg mL^{-1},

to (c) 0.1 mg mL^{-1}, to (d) 0.02 mg mL^{-1} and to (e) 0.0025 mg mL^{-1}. The modeled self-assembled pattern (called "Model") based on our described model is given on the right side of the corresponding experimental Type I, II, III-i. III-ii and IV pictures. All the parameters used in the simulations are provided in ESI,† Part 3, Table S1.

continuous self-assembly regime. This too is observed experimentally. One also observes that, in the microglobule regime (Fig. 3e, Type IV), at an enzyme concentration close to the continuous/microglobule transition, there are many microglogules. As one decreases the enzyme concentration (always at fixed Fmoc-FF*p*Y concentration of 1.2 mg mL^{-1}), the number of microglobules per picture decreases but their size increases. As the enzyme concentration becomes even smaller than 0.0025 mg mL^{-1}, one gets images with very few, sometimes only one or even no microglobule left. This is in accordance with the predictions of our model as well (Fig. S5, ESI†).

In the Type II or III profile regime (Fig. 3b and c), by keeping the enzyme concentration fixed ([AP] = 0.3 mg mL^{-1}) and decreasing the Fmoc-FF*p*Y concentration from 5, 2.5, 1.25 down to 0.6 mg mL^{-1}, one gets the experimental results shown in Fig. 4a: the location of the second self-assembly maximum is quite identical highlighting its independence from the peptide concentration. The depletion zone between the two maxima remains unchanged. Only the depth over which the second maximum of self-assembled peptides extends is greater when c_{PP} is higher. These results are well reproduced by our model at low peptide concentrations (Fig. 4b). But, at low peptide concentrations, one is very sensitive to what happens in the solution and at the gel–solution interface. Actually, what happens in the solution is not intended to be well reproduced by our model because of eventual convection phenomena occurring at the solution/air interface and that are herein not taken into account. Previous experimental results have shown that by decreasing the Fmoc-FF*p*Y concentration, one increases the enzyme concentration at which the continuous/microglobule transition takes place (Table 1). This trend is also well anticipated by our model.[28]

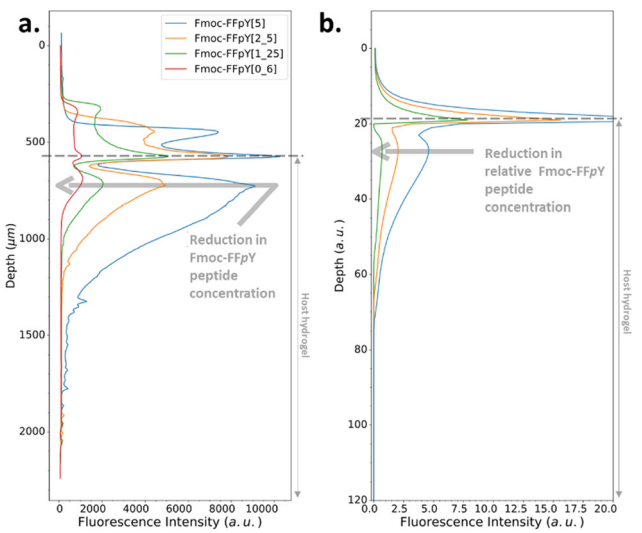

Fig. 4 (a) Experimentally recorded cross-section profiles measured within the AP-HPMC host gel showing the spatial location of Fmoc-FFY peptide self-assembly pattern thanks to the ThT fluorescence intensity emission observed by CLSM. The concentration of the precursor peptide Fmoc-FF*p*Y is varied from 5 (blue curve), 2.5 (orange curve), 1.25 (green curve) down to 0.6 (red curve) mg mL^{-1} when the concentration of AP embedded in the AP-HPMC host gel is kept constant at 1 mg mL^{-1}. (b) Simulated patterns obtained in the same conditions using equivalent relative Fmoc-FF*p*Y and AP (all the parameters used in the simulations are provided in ESI,† Part 3, Table S1).

Table 1 Enzyme concentration in the AP-HPMC host gel at which the continuous/microglobule transition is experimentally observed for different peptide concentrations.[28] It must be noted that all experiments were performed with the same batches of peptides and enzymes

[Fmoc-FF*p*Y] (mg mL^{-1})	5	2	1
[AP] (μg mL^{-1})	<1.2	1.2	5

We have also investigated the influence of the CC of the peptide hydrogelator on the resulting experimental self-assembled pattern, and its comparison with the simulated pattern. The CC is a unique feature specific to the chemical structure of the self-assembling entity considered. Thus, we have designed a new precursor peptide, close to Fmoc-FF*p*Y, by adding a phenylalanine residue on the N-term part resulting in the Fmoc-FFF*p*Y precursor peptide (Fig. 2a). This compound is still soluble in water and sensitive to the hydrolytic action of AP leading to Fmoc-FFFY self-assembled nanofibers (8 nm diameter) as observed by TEM (Fig. 2a and Fig. S4, ESI†). Because of the more important hydrophobic part of Fmoc-FFFY compared to Fmoc-FFY, its CC is roughly ten times lower, *i.e.* 2.5 μM for Fmoc-FFFY and 20 μM for Fmoc-FFY (Fig. S2, ESI†). For a Fmoc-FFF*p*Y solution at 1 mg mL^{-1} diffusing through the AP-HPMC host gel containing 0.012 mg mL^{-1} of AP, one observes a self-assembled Fmoc-FFFY pattern of Type II (Fig. 5a). Type II is characterized by a very narrow depletion zone and thus two self-assembled peptide areas very close one to each other. A pattern profile of Type III can be observed for a Fmoc-FFF*p*Y solution using less than 0.012 mg mL^{-1} of AP. Indeed, by decreasing the enzyme concentration in the AP-HPMC host gel from 0.1, 0.05, 0.025, 0.012 down to 0.0012 mg mL^{-1}, we observed a slight, but significant, shift of the second maximum in-depth in the material, becoming less intense and finally resulting in the appearance of microglobules (spikes present in the graph) corresponding to a transition from the Type III-i to the Type III-ii profile, as simulated (Fig. 5b). For comparison, the same continuous/microglobule transition takes place at an AP concentration above 0.005 mg mL^{-1} for Fmoc-FF*p*Y solution (1 mg mL^{-1}). These results indicate that when decreasing the CC, the self-assembly profile sequence (profile Type I to profile Type IV) is shifted towards lower enzyme concentrations. This experimental observation is thus also predicted by our model.

All the experiments reported so far were performed by adding a given volume of solution on top of the host gel of constant volume. In order both to verify the influence of the volume of solution and to evaluate the robustness of our model, by keeping all the other parameters constant, we have

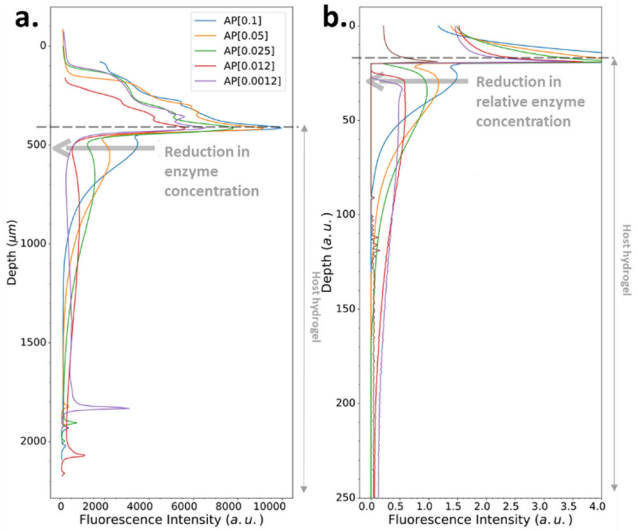

Fig. 5 (a) Experimentally recorded cross-section profiles measured within the AP-HPMC host gel showing the spatial location of Fmoc-FFFY peptide self-assembly pattern thanks to the ThT fluorescence intensity emission observed by CLSM. The concentration of the precursor peptide Fmoc-FFF*p*Y solution is kept at 1 mg mL^{-1} in each case, but the AP concentration embedded in the host hydrogel is varied from 0.1, 0.05, 0.025, 0.012 down to 0.0012 mg mL^{-1}. (b) Simulated patterns obtained in the same conditions using relative Fmoc-FFF*p*Y and AP concentrations (all the parameters used in the simulations are provided in ESI,† Part 3, Table S1).

performed experiments by adding a volume of solution that is twice that previously added in this study. Fig. 6a shows that this

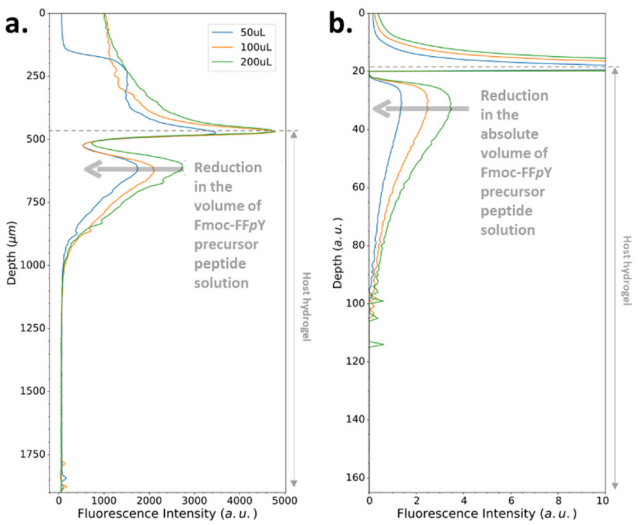

Fig. 6 (a) Experimentally recorded cross-section profiles measured within the AP-HPMC host gel showing the spatial location of Fmoc-FFFY peptide self-assembly pattern thanks to the ThT fluorescence intensity emission observed by CLSM. The concentration of the precursor peptide Fmoc-FFF*p*Y solution is kept at 1 mg mL^{-1} in each case, but the volume solution is changed from 50, 100 up to 200 μL. The AP concentration embedded in the AP-HPMC host gel is 0.1 mg mL^{-1}. (b) Simulated patterns obtained in the same conditions using relative Fmoc-FF*p*Y volume solutions (all the parameters used in the simulations are provided in ESI,† Part 3, Table S1).

does not change the extension of the depletion zone and the location of the self-assembly maximum in the gel with respect to the interface, as simulated (Fig. 6b).

Finally, we have also changed the chemical nature of the host gel in order to verify that the observed self-assembly profiles are not host-gel dependent. We replaced the cellulose-based host gel (HPMC) by a hyaluronic acid (HA) based gel in which HA was covalently reticulated in the same way as the HPMC gel (see Material and methods section above). The same enzyme/peptide was used and the AP enzymes were incorporated in the HA in a similar way than in HPMC. We performed experiments at high and low enzyme concentrations and recovered a continuous self-assembly profile with two maxima and a depletion zone at high enzyme concentration and self-assembly globules at low enzyme concentration (see Part 5 in ESI,† for more details). This proves the independence of the observed features from the host gel.

Influence of the different parameters of the model on the peptide self-assembly profile. The model that we have developed relies on different parameters. Some of them were introduced to directly account for experimental observation. This is the case of the enzyme adsorption constant k_{ea} and of the dephosphorylated peptide Fmoc-FFY "desorption" constant k_{ad}. It is also the case of the initial enzyme distribution profile. The self-assembly profiles shown above were obtained by a tedious trying and error procedure and can certainly be optimized. Yet, due to the large number of parameters and to the time required to generate a self-assembly profile, it seems impossible with conventional computer facilities to use an optimization procedure to determine optimized parameters. We now want to shortly discuss the influence of some of these parameters on the resulting self-assembly profiles.

The model proposed in the present work contains several parameters. The question arises as to whether their number could be reduced while retaining the capability to capture the most striking of the experimental observations namely the non-monotonous self-assembly profile at high enzyme concentration and the transition from a continuous to a globule profile when the enzyme concentration is lowered? The profiles shown above were all obtained by assuming that the critical aggregation concentration (CC) is 0 in the solution and the enzyme activity is 5 times higher in the solution than in the gel. The constants k_{ad} and k_{ea} were different from zero (see Part 4, Table S1 in ESI,† for the values of all these constants). From the large numbers of trials performed in order to get a reasonable set of parameters accounting qualitatively for the observed features, it comes out that it is necessary that the CC be smaller in the solution than in the gel. We have thus performed simulations where CC remains equal to zero in the solution but we put $k_{ad} = 0$ and $k_{ea} = 0$ (no "desorption" of peptides from the self-assembled structure and no adsorption of enzymes on the self-assembled structure). It appears that most of the observed features are reproduced qualitatively (Fig. S6A, ESI†). For low enzymes concentrations corresponding to profile of Type III-ii, it appears that the depletion zone is enlarged when $k_{ea} = 0$.

We have then repeated the simulations by setting the enzyme activity equal in the solution and in the gel but we kept CC = 0 in the solution (Fig. S6B, ESI†) ($r_{k_e} = 1$). Here too, one observes self-assembly profiles that are very close one from each other over the entire enzyme concentration range when the enzymatic activity is the same in the solution and in the gel compared to the case where it is 5 times higher in the solution than in the gel. One can nevertheless remark that the profiles are slightly more "peaked" at the secondary maximum when k_E is the same in the solution and in the gel and thus reproduces slightly less accurately the shape of the observed experimental profile. However, because our model is not intended to reproduce the exact shape of the self-assembly profiles but rather the main observed features, one can conclude that the same enzymatic reaction constant can be adopted in the solution and in the gel.

We have also increased the CC in the solution from zero up to its value in the gel for a given value of the enzyme concentration corresponding to a Type III profile. This was done by taking the same enzymatic activity in the solution and in the gel. It comes out that increasing the CC in the solution, all other parameters remaining fix, decreases the extension of the depletion zone which disappears when CC in solution becomes very close to its value in the gel (Fig. S6C, ESI†). Remarkably the self-assembly profile is not greatly affected after the depletion zone in the gel.

Next, we have chosen the same value of CC in the solution and in the gel and increased the enzyme activity in the solution compared to that in the gel. No depletion zone is observed at the gel/solution interface (Fig. S6D, ESI†). This shows that a smaller value of CC in the solution than in the gel is necessary to account for the depletion zone observed in the experimental self-assembly profiles.

The nucleation process is characterized by a rapid increase of the nucleation rate when the precursor concentration exceeds a critical value. Even if nucleation theories predict quite accurately the critical degree of supersaturation (here CC) at which nucleation starts, they are usually far from predicting accurately the nucleation rate. We thus assumed that the exact mathematical form of the random function $r(c_{PH})$ is not crucial to predict qualitatively most of the observed self-assembly features as long as its value increases rapidly when the precursor concentration c_{PH} approaches, then exceeds CC. The random function $r(c_{PH})$, using eqn (7), was chosen because its variation around CC can easily be tuned by the factor P_1. The effect of this parameter was investigated (Fig. S6E, ESI†). Keeping all other parameters fix and decreasing P_1 makes the self-assembly profile evolving from a Type III-i profile (for the used parameters) to a profile of Type III-ii and finally a profile presenting multiple self-assembly areas. It is interesting to note the "unphysical" shape of these zones with a maximum at both extremities. This feature is observed in fully deterministic models developed to describe Liesegang patterns and shows the importance of incorporating stochasticity in the Liesegang models to account in correct way for the experimental results.[43]

We also tested the random function $\frac{\delta t}{\tau}\left(\frac{c_{PH}}{CC}\right)^n$. This function is used in the non-classical nucleation theory to describe the nucleation of amyloid fibrils.[44] We have chosen $n = 8$ and $n = 4$. Here we cannot set CC equal to 0 in the solution. We have thus set it to 0.1 times its value in the gel. Two series of simulations were run with $n = 8$: one with the same enzymatic activity in the solution and in the gel (Fig. S6F, ESI†) and another series where the enzymatic activity was 5 times higher in the solution than in the gel (Fig. S6G, ESI†). With $n = 4$ simulations were run only with an enzymatic activity 5 times higher in the solution than in the gel. As shown in ESI† (Fig. S6F and G), with this random function we also capture qualitatively the observed evolution of the self-assembly profile as a function of the enzyme concentration both with $n = 8$ and $n = 4$.

Conclusion

In summary, we have developed a robust model that predicts the features of a chemical system composed of precursor peptides diffusing within a host gel containing enzymes that transform the precursors into hydrogelators. These hydrogelators self-assemble when they reach a concentration close to the critical concentration to form self-assemblies that are not able to diffuse. This mechanism leads to self-assembled structures ranging from continuous profiles to individual microglobules that are predicted by the model. Our model relies on parameters related to diffusion coefficients, reaction constants, initial concentrations of precursor peptide and enzyme. It takes the stochastic nature of the nucleation process into account which is essential to describe the continuous-to-microglobule transition. Our model, and in particular the way how stochasticity is introduced, can be extended to all systems where reaction/diffusion/nucleation processes take place. In the future, it would be of great interest to develop chemical systems where most of the parameters entering the model could be determined experimentally. Knowing the value of the parameters would allow to refine the random function to predict more quantitatively the exact shape of the self-assembly profile. Refining the random function would also give new information on the initial steps of the nucleation process, a question still under debate.

Conflicts of interest

There are no conflicts to declare.

Acknowledgements

We gratefully acknowledge the financial support from "Agence Nationale de la Recherche" (EASA, ANR-18-CE06-0025-03 and CASH, ANR-21-CE06-0033) and the "Fondation Jean-Marie Lehn", "ITI Chimie des Systèmes Complexes" (Project PSc-CSC-0008). The ICS characterization and microscopy platforms CARMAC & PLAMICS are acknowledged. We thank the mechanical support from ICS and Karim Benmlih (INSERM U1121) for the design and fabrication of the experimental setups. Dr Jean-Marc Strub is acknowledged for mass analyses.

Notes and references

1 Z. Yang, H. Gu, D. Fu, P. Gao, J. K. Lam and B. Xu, *Adv. Mater.*, 2004, **16**, 1440.

2 A. R. Hirst, S. Roy, M. Arora, A. K. Das, N. Hodson, P. Murray, S. Marshall, N. Javid, J. Sefcik, J. Boekhoven, J. H. van Esch, S. Santabarbara, N. T. Hunt and R. V. Ulijn, *Nat. Chem.*, 2010, **2**, 1089; R. J. Williams, J. Gardiner, A. B. Sorensen, S. Marchesan, R. J. Mulder, K. M. McLean and P. G. Hartley, *Aust. J. Chem.*, 2013, **66**, 572.

3 C. Muller, A. Ontani, A. Bigo-Simon, P. Schaaf and L. Jierry, *Adv. Colloid Interface Sci.*, 2022, **304**, 102660.

4 R. J. Williams, A. M. Smith, R. Collins, N. Hodson, A. K. Das and R. V. Ulijn, *Nat. Nanotechnol.*, 2009, **4**, 19.

5 J. Zhan, Y. Cai, S. Ji, S. He, Y. Cao, D. Ding, L. Wang and Z. Yang, *ACS Appl. Mater. Interfaces*, 2017, **9**, 10012.

6 R. J. Williams, T. E. Hall, V. Glattauer, J. White, P. J. Pasic, A. B. Sorensen, L. Waddington, K. M. McLean, P. D. Currie and P. G. Harthley, *Biomaterials*, 2011, **32**, 5304; M. Hughes, S. Debnath, C. W. Knapp and R. V. Ulijn, *Biomater. Sci.*, 2013, **11**, 1138.

7 M. P. Conte, J. Kishore Sahoo, Y. M. Abdul-Haija, K. H. Aaron Lau and R. V. Ulijn, *ACS Appl. Mater. Interfaces*, 2018, **10**, 3069.

8 J. Rodon Fores, M. Criado-Gonzalez, A. Chaumont, A. Carvalho, C. Blanck, M. Schmutz, C. A. Serra, F. Boulmedais, P. Schaaf and L. Jierry, *Angew. Chem., Int. Ed.*, 2019, **58**, 18817.

9 X. Du, J. Zhou, J. Shi and B. Xu, *Chem. Rev.*, 2015, **115**, 13165; B. Yang, D. J. Adams, M. Marlow and M. Zelzer, *Langmuir*, 2018, **34**, 15109.

10 Z. Yang, G. Liang, Z. Guo, Z. Guo and B. Xu, *Angew. Chem., Int. Ed.*, 2007, **46**, 8216; J. Li, J. Shi, J. Zhou, J. E. Medina, R. Zhou, D. Yuan, C. Yang, H. Wang, Z. Yang, J. Liu, D. M. Dinulescu and B. Xu, *Angew. Chem., Int. Ed.*, 2015, **54**, 13307; R. A. Pires, Y. M. Abdul-Haija, D. S. Costa, R. Novoa-Carballal, R. L. Reis, R. V. Ulijn and I. Pashkuleva, *J. Am. Chem. Soc.*, 2015, **137**, 576; Z. Feng, H. Wang, R. Zhou, J. Li and B. Xu, *J. Am. Chem. Soc.*, 2017, **139**, 3950.

11 S. Kondo and T. Miura, *Science*, 2010, **329**, 1616; S. Soh, M. Byrska, K. Kandere-Grzybowska and B. Grzybowski, *Angew. Chem., Int. Ed.*, 2010, **49**, 4170.

12 M. Lovrak, W. E. J. Hendriksen, C. Maity, S. Mytnyk, V. van Steijn, R. Eelkema and J. H. van Esch, *Nat. Commun.*, 2017, **8**, 15317.

13 M. Lovrak, W. E. Hendriksen, M. T. Kreutzer, V. van Steijn, R. Eelkema and J. H. van Esch, *Soft Matter*, 2019, **15**, 4276.

14 M. Lovrak, S. J. Picken, R. Eelkema and J. H. van Esch, *ChemNanoMat*, 2018, **4**, 772.

15 J. Ruiz-Olles and D. K. Smith, *Chem. Sci.*, 2018, **9**, 5541.

16 P. Ravarino, S. Panja and D. J. Adams, *Macromol. Rapid Commun.*, 2022, **43**, 2200606.

17 I. Ziemecka, G. J. M. Kopper, A. G. L. Olive and J. H. van Esch, *Soft Matter*, 2013, **9**, 1556; A. G. L. Olive, N. H. Abdullah, I. Ziemecka, E. Mendes, R. Eelkema and J. H. van Esch, *Angew. Chem., Int. Ed.*, 2014, **53**, 4132; J. Rodon Fores, M. L. M. Mendez, X. Mao, D. Wagner, M. Schmutz, M. Rabineau, P. Lavalle, P. Schaaf, F. Boulmedais and L. Jierry, *Angew. Chem., Int. Ed.*, 2017, **56**, 15984.

18 D. Spitzer, V. Marichez, G. J. M. Formon, P. Besenius and T. M. Hermans, *Angew. Chem., Int. Ed.*, 2018, **57**, 11349.

19 L. Schlichter, C. C. Piras and D. K. Smith, *Chem. Sci.*, 2021, **12**, 4162.

20 C. Tangsombun and D. K. Smith, *J. Am. Chem. Soc.*, 2023, **145**, 24061.

21 H. S. Cooke, L. Schlichter, C. C. Piras and D. K. Smith, *Chem. Sci.*, 2021, **12**, 12156.

22 M. Criado-Gonzalez, J. Rodon Fores, D. Wagner, A. P. Schröder, A. Carvalho, M. Schmutz, E. Harth, P. Schaaf, L. Jierry and F. Boulmedais, *Chem. Commun.*, 2019, **55**, 1156.

23 M. Criado-Gonzalez, B. Loftin, J. Rodon Fores, D. Vautier, L. Kocgozlu, L. Jierry, P. Schaaf, F. Boulmedais and E. Harth, *J. Mater. Chem. B*, 2020, **8**, 4419.

24 M. Criado-Gonzalez, J.-Y. Runser, A. Carvalho, F. Boulmedais, P. Weiss, P. Schaaf and L. Jierry, *Polymer*, 2022, **261**, 125398.

25 W. Wang, J. Qian, A. Tang, L. Ann, K. Zhong and G. Liang, *Anal. Chem.*, 2014, **86**, 5955.

26 C. Vigier-Carrière, T. Garnier, D. Wagner, P. Lavalle, M. Rabineau, J. Hemmerlé, B. Senger, P. Schaaf, F. Boulmedais and L. Jierry, *Angew. Chem., Int. Ed.*, 2015, **54**, 10198.

27 J. Y. Runser, M. Criado-Gonzalez, F. Fneich, M. Rabineau, B. Senger, P. Weiss, L. Jierry and P. Schaaf, *J. Colloid Interface Sci.*, 2022, **620**, 234.

28 J. Y. Runser, F. Fneich, B. Senger, P. Weiss, L. Jierry and P. Schaaf, *J. Colloid Interface Sci.*, 2023, **633**, 876.

29 F. F. Runge, *Self-Edited*, 1855, 69; R. Liesegang, *Naturwiss. Wochenschr.*, 1896, **11**, 353; R. Sultan, P. Ortoleva, F. DePasquale and P. Tartaglia, *Earth-Sci. Rev.*, 1990, **29**, 163; H. Nabika, M. Itatani and I. Lagzi, *Langmuir*, 2020, **36**, 481.

30 J. Rodon Fores, A. Bigo-Simon, D. Wagner, M. Payrastre, C. Damestoy, L. Blandin, F. Boulmedais, J. Kelber, M. Schmutz, M. Rabineau, M. Criado-Gonzalez, P. Schaaf and L. Jierry, *Polymers*, 2021, **13**, 1793.

31 D. Mertz, C. Vogt, J. Hemmerlé, J. Mutterer, V. Ball, J.-C. Voegel, P. Schaaf and P. Lavalle, *Nat. Mater.*, 2009, **8**, 731.

32 C. Trojani, P. Weiss, J.-F. Michiels, C. Vinatier, J. Guicheux, G. Daculsi, P. Gaudray, G. F. Carle and N. Rochet, *Biomaterials*, 2005, **26**, 5509.

33 K. Flegeau, C. Toquet, G. Rethore, C. d'Arros, L. Messager, B. Halgand, D. Dupont, F. Autrusseau, J. Lesoeur, J. Veziers, P. Bordat, A. Bresin, J. Guicheux, V. Delplace, H. Gautier and P. Weiss, *Adv. Healthcare Mater.*, 2020, **9**, 2000981.

34 H. Nabika, M. Itatani and I. Lagzi, *Langmuir*, 2020, **36**, 481.

35 B. Chopard, P. Luthi and M. Droz, *J. Stat. Phys.*, 1994, **76**, 661.

36 B. Chopard, P. Luthi and M. Droz, *Phys. Rev. Lett.*, 2003, **371**, 321.

37 T. Antal, M. Droz, J. Magnin, A. Pekalski and Z. Racz, *J. Chem. Phys.*, 2001, **114**, 3770.

38 F. Izsak and I. Lagzi, *Chem. Phys. Lett.*, 2003, **371**, 321.

39 I. T. Bensemann, M. Fialkowski and B. A. Grzybowski, *J. Phys. Chem. B*, 2005, **109**, 2774.
40 C. W. Pan, Q. Y. Gao, J. X. Xie, Y. Xia and I. R. Epstein, *Phys. Chem. Chem. Phys.*, 2009, **11**, 11033.
41 F. Izsak and I. Lagzi, *J. Chem. Phys.*, 2004, **120**, 1837.
42 K. Tsushima, M. Itatani, Q. Fang and H. Nabika, *Langmuir*, 2023, **39**, 249.
43 A. A. Polezhaev and S. C. Müller, *Chaos*, 1994, **4**, 631.
44 T. C. T. Michaels, D. Qian, A. Šarić, M. Vendruscolo, S. Linse and T. P. J. Knowles, *Nat. Rev. Phys.*, 2023, **5**, 379.

